Polymer Journal (2016) 48, 341–350

www.nature.com/pj

FOCUS REVIEW

Surface-initiated atom transfer radical polymerization for applications in sensors, non-biofouling surfaces and adsorbents

Chih-Feng Huang

Surface-initiated reversible-deactivation radical polymerization (SI RDRP) has become a powerful tool for the preparation of functional surfaces and interfaces to match the needs of applications. This focused review describes how surface properties can be manipulated by combining surface-initiated atom transfer radical polymerization (SI ATRP) and the very-large-scale integration (VLSI) lithography process. These fabricated surfaces, which are solvent-responsive or bio-inert/bioactive, have been applied to volatile organic compound (VOC) sensors and to non-biofouling/cell-growing surfaces. The functionalization of renewable resources and how SI ATRP is being extended toward the applications of high-performance adsorbents are also discussed.
Polymer Journal (2016) **48,** 341–350; doi:10.1038/pj.2016.24; published online 24 February 2016

INTRODUCTION

Various living polymerization processes[1–9] have been investigated thoroughly in recent decades, leading to robust tools that have enabled the innovation of unprecedented surface-functionalized nanomaterials through modification or grafting onto/from the peripheral groups. Proceeding polymerizations from solid-support surfaces and surface-initiated reversible-deactivation radical polymerizations (SI RDRPs) have become major strategies to meet the demanding requirements in many applications. SI RDRPs enable surface-initiated polymerizations with a wide range of functional monomers, providing excellent control over the molecular weight, narrow molecular weight distribution and high graft density of polymer brushes. These features allow significant manipulations of the surface properties, including hydrophobicity/hydrophilicity, bio-inert/bioactive and responsiveness. The most widely studied SI RDRP systems include surface-initiated atom transfer radical polymerization (SI ATRP),[10,11] surface-initiated nitroxide-mediated radical polymerization[12] and surface-initiated reversible addition-fragmentation chain transfer (SI RAFT) polymerization,[13,14] among others.[15,16] Recently, Chilkoti and colleagues[17] conducted SI ATRP of poly(ethylene glycol) methacrylate (PEGMA) combined with lithography to fabricate micro- and nanoscale patterned surfaces in large areas with high throughput and repeatability while preventing protein and cell adhesion from the poly(poly(ethylene glycol) methacrylate) (PPEGMA) brush. Klok and colleagues[18] demonstrated the concept of the low-density polyethylene surface with specific adhesion of cells by sequential SI ATRP of PEGMA and attachment of the GGGRGDS peptide ligand on PPEGMA brushes. The surface with PPEGMA brushes had anti-biofouling properties, but the surface with PPEGMA-GGGRGDS brushes enabled human umbilical vein endothelial cells (HUVECs) to adhere. Several critical reviews[19–25] have reported anti-biofouling/cell-adhesion interfaces using SI RDRPs. These reports indicated recent breakthroughs in the smart control of non-biofouling/cell-adhesion interfaces using SI RDRPs.

Combining these creative polymerization techniques with eco-friendly materials should enhance the environmental sustainability of the resulting materials. Polysaccharides (for example, alginate, chitosan, cellulose and starch) and their derivatives are widely used because of their low-cost, eco-friendliness, renewability and attractive physical characteristics. For example, cellulose, which is readily acquired from crops and wood, possesses good crystallinity, mechanical strength, renewability and biodegradability. Furthermore, nanosized celluloses (generally known as cellulose nanofibrils[26] and classified into four main types: nanofibrillated cellulose, cellulose nanowhisker/nanocrystal cellulose, bacterial nanocellulose and 2,2,6,6-tetramethylpiperidine-1-oxyl (TEMPO)-oxidized cellulose nanofiber (TOCN)) can possess high-performance physical properties. Using SI living polymerizations to develop unique cellulose nanofibril nanomaterials derived from natural resources is a long-term goal of macromolecular engineering; nevertheless, only a few related studies have been demonstrated.[27–33]

Several simple chemical and physical approaches (and their combinations) are available for manipulating surface properties. In this review, we first focus on the scope of surfaces/interfaces available using SI ATRP and lithography processes, providing patterning surfaces for the applications of non-biofouling/cell-growing interfaces and solvent-responsive materials. We then describe the effective approaches of SI ATRP and TEMPO-mediated oxidation for the

Department of Chemical Engineering, National Chung Hsing University, Taichung, Taiwan
Correspondence: Dr C-F Huang, Department of Chemical Engineering National Chung Hsing University, Eng Bld 3, 250 Kuo Kuang Road, Taichung 402, Taiwan.
E-mail: HuangCF@dragon.nchu.edu.tw
Received 23 November 2015; revised 11 January 2016; accepted 21 January 2016; published online 24 February 2016

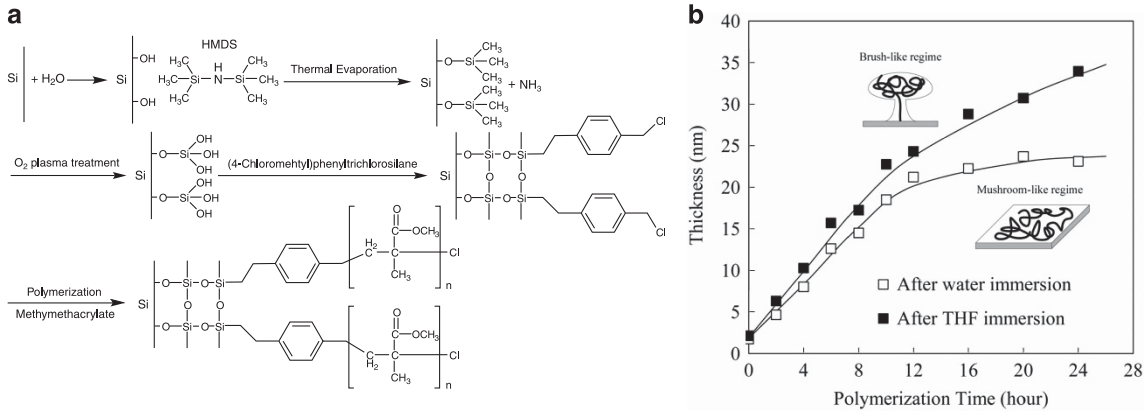

Figure 1 (**a**) Preparation of PMMA brushes through surface modifications and SI ATRP on Si wafers. (**b**) Dependence of the thickness of the PMMA layer, grown by SI ATRP from Si wafers and immersed in water or THF, on the polymerization time.

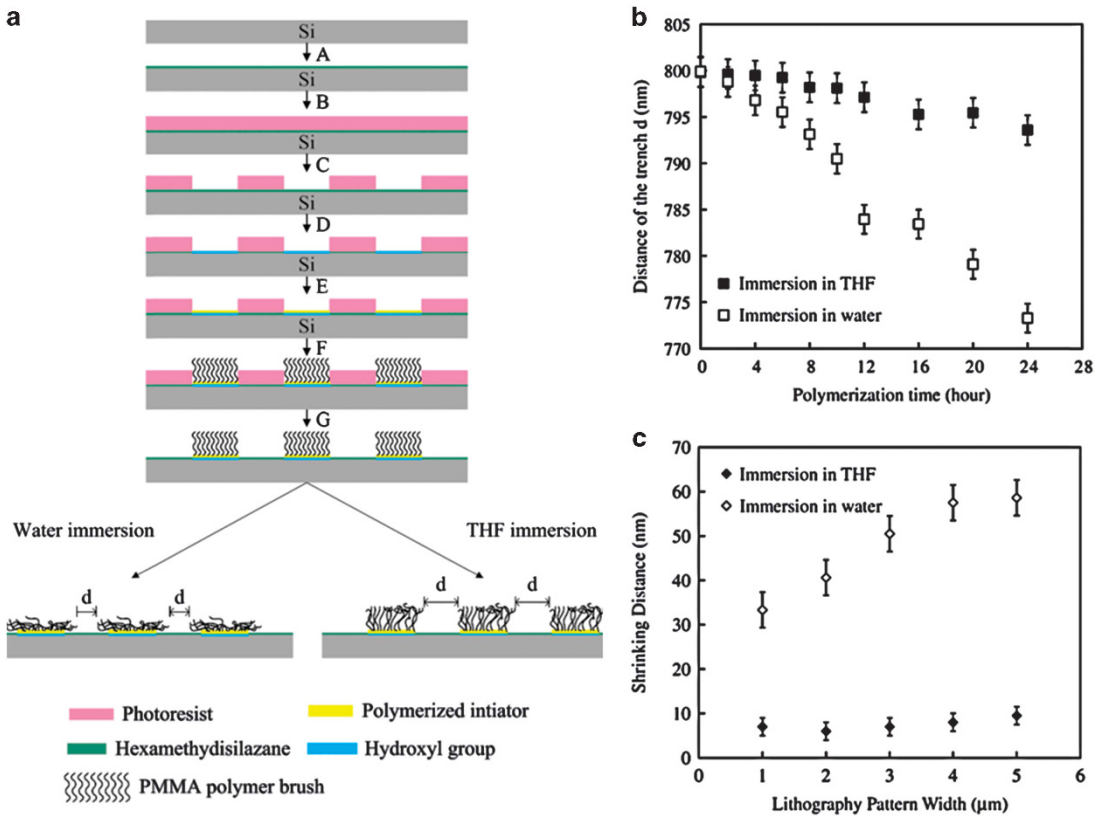

Figure 2 (**a**) VLSI process: (A) treatment of HMDS on Si wafer; (B) photoresist spin-coating; (C) lithographic patterning on the photoresist; (D) using O_2 plasma to modify the exposed regions; (E) selective attachment of initiator, CMPCS, onto the bare regions of the Si surface; (F) SI ATRP of MMA from the Si-CMPCS surface; (G) removal of photoresist. (**b**) Changes in the trenches (i.e., d) of the PMMA brushes immersed in water and THF plotted with respect to the polymerization time. (**c**) Shrinkage based on the lithography trench width.

application of high-performance adsorbents. We provide an overview that focuses on surface modifications, surface-initiated polymerization and surface molecular level association, rather than a detailed study.

APPLICATIONS FOR VOC SENSORS AND BIO-INTERFACES VIA SI ATRP FROM SOLID SUPPORTS

Since Whitesides *et al.*[34] first demonstrated the significant suppression of protein adsorption by self-assembled monolayers, the effective surface/interface modification of organic/inorganic substrates has found great applicability. The major drawback of self-assembled monolayers, however, is their instability under harsh conditions. The more recent fabrication of polymer brushes on solid supports has provided an alternative robust approach for developing surfaces/interfaces displaying a wide range of physical and chemical properties. Polymer brushes fabricated through SI RDRP are more tolerant of harsh conditions and allow the fabrication of (block co)polymer brushes with controlled grafting densities and thicknesses.[11,25] In this section, we focus on the use of SI ATRP. Figure 1a depicts a strategy for the fabrication of patterned poly(methyl methacrylate) (PMMA)

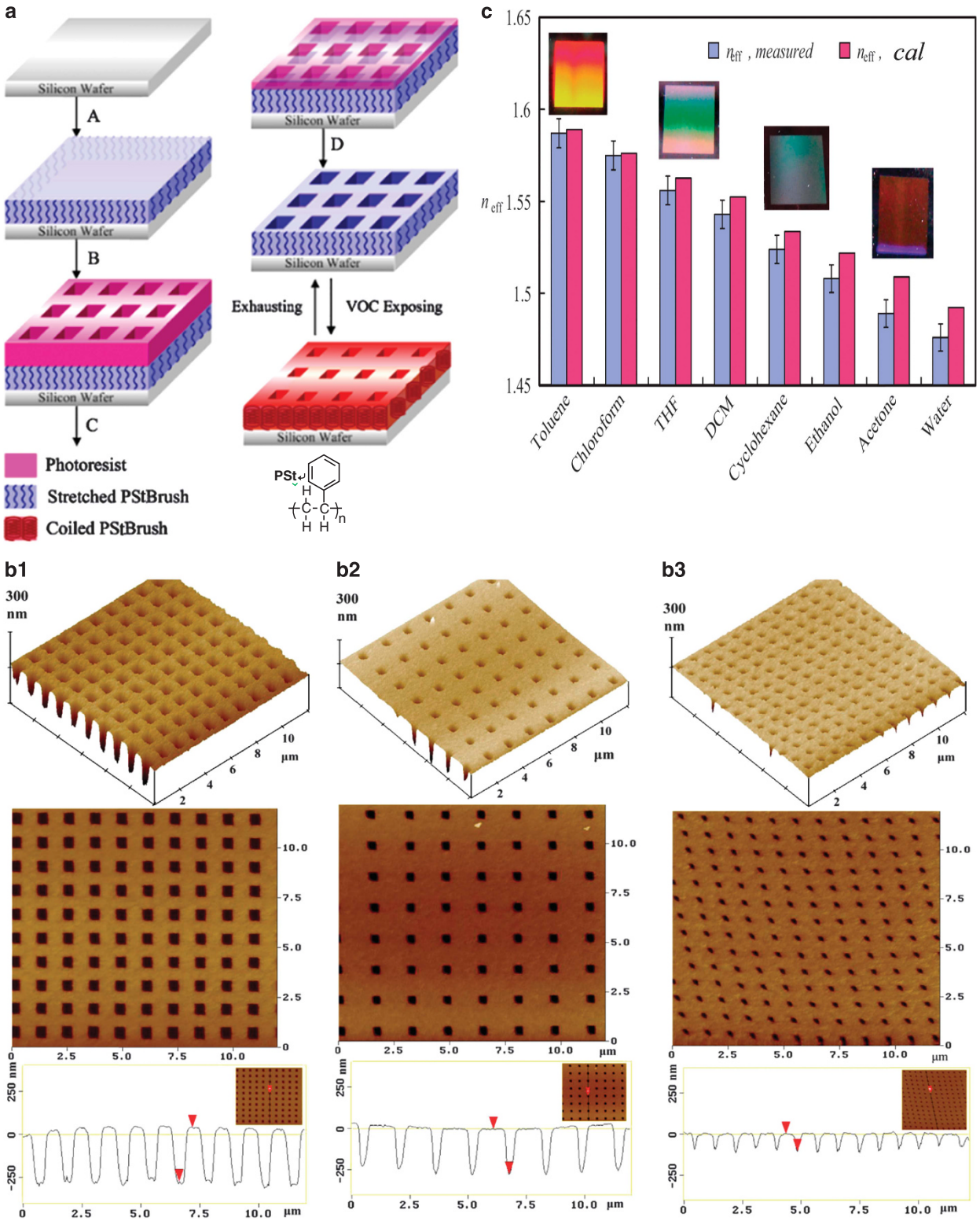

Figure 3 (**a**) Fabrication of 2DPCGs having a tethered PSt layer ((A) SI ATRP of styrene from Si wafer; (B) spin-coating photoresist and patterning by e-beam lithography to obtain 2DPCG on the surface; (C) transferring the 2DPCG pattern to the tethered PSt layer; (D) removing photoresist) and their applications in VOC sensing. (**b**) AFM topographic images (3D, top and cross-sectional views) of a PSt-tethered 2DPCG surface (**b1**) in the dry film state and (**b2**, **b3**) after VOC exposure to (**b2**) dichloromethane (DCM) and (**b3**) toluene. (**c**) Measured and calculated values of n_{eff} of a 2DPCG with a tethered PSt layer after VOC exposure to various solvents.

brushes on a Si wafer.[35] SI ATRP was performed with MMA/CuBr/PMDETA = 2800/1/1 and an initiator-immobilized Si wafer (that is, Si-CMPCS) in toluene at 85 °C ($[MMA]_0 = 3.9$ M). X-ray photoelectron spectroscopy and contact angle (CA) measurements confirmed the surface modifications. Figure 1b displays the thicknesses of the PMMA brushes grafted from the Si-CMPCS surfaces after various polymerization times and after immersing in water or tetrahydrofuran (THF). Linear increases in the thickness of the PMMA layer occurred for polymerization times within 12 h after immersion in either solvent. For polymerizations longer than 12 h, the thickness of the PMMA layer reached a plateau in the case of water immersion, providing a so-called mushroom-like topology for the PMMA brushes. In the case of THF immersion, the thickness of the PMMA layer increased as the polymerization time extended beyond 12 h, indicating the formation of a brush-like topology for the PMMA brushes. Using atomic force microscopy (AFM), the PMMA brush layers immersed in water (that is, poor solvent) revealed a distinctive overlayer after immersion because the mushroom-like structures formed on the surface resulted from a collapse of the PMMA chains.[36] By contrast, the PMMA brush layers immersed in THF (that is, good solvent) revealed the formation of islands that presumably arose from the brush-like structure. These observations confirmed that solvents can affect the topologies of grafted polymer brushes.

The combination of SI RDRPs and the lithographic process in the fabrication of 'smart' surfaces has recently been reviewed.[37–39] Using the very-large-scale integration (VLSI) process, our next attempt was to comprehend the morphological differences that occurred to the surface-patterned structures upon changing in solvent.[40] The VLSI processes to fabricate patterned PMMA layers through the use of SI ATRP and VLSI processing are illustrated in Figure 2a. Measured by AFM, the trench distances between the PMMA brushes (that is, d in Figure 2a) after water and THF immersion increased linearly with respect to the polymerization time (Figure 2b). In the case of immersion in water (hollow squares), the PMMA brushes stretched laterally with increasing polymerization time, resulting in shrinking of the trench distances due to the formation of the mushroom-like morphology of the PMMA brushes. By contrast, in the case of immersion in THF (solid squares), the trench distances between the PMMA brushes were affected in a slightly different manner. The formation of a brush-like regime of PMMA brushes was anticipated. The shrinking distance (defined as the *lithography pattern width* minus the *observed trench distance*) increased with increasing lithography pattern width (Figure 2c) due to the presence of various thicknesses of PMMA brushes with different graft densities. Thus, the thicknesses and trench distances of the patterned PMMA brushes can be controlled significantly by means of immersing the brushes in solvents with different polarities.

The use of polymers as building blocks attached to solid supports can lead to 'smart' surfaces manipulated through conformational changes of the polymer chains in response to environmental conditions (for example, pH, temperature and solvent). We fabricated two-dimensional periodic concave gratings (2DPCG) featuring a patterned polystyrene (PSt) layer through the use of SI ATRP and VLSI processing (Figure 3a).[41] For the preparation of PSt brushes, St, CuBr, $CuBr_2$ and PMDETA were added to anhydrous toluene. After polymerization, the wafer was placed in a Soxhlet apparatus to clean the surface. This solvent polarity-responsive 2DPCG device can function as a new type of sensor for volatile organic compounds (VOCs), according to the different swelling behavior of PSt under various VOC environments. Figure 3b presents topographic AFM images of the distinctive square-hole shrinkage of the 2DPCG surface before and after exposure to dichloromethane and toluene as representative VOCs. Figure 3b1 reveals a square size of approximately 600 nm and a depth of approximately 267.5 nm. After exposure to dichloromethane (Figure 3b2), the square-hole size and depth became 443 and 242 nm, respectively. After exposure to toluene (Figure 3b3), the size and depth changed significantly to 251 and 104 nm, respectively, because toluene is a very good solvent for PSt swelling. The reversibility of this swelling/deswelling behavior suggests the practicality of applying such surfaces to VOC detection. We also examined 2DPCGs with PSt-tethered layers for VOC sensing through measurements of the differences in the effective refractive index (n_{eff}) caused by the morphological changes in response to exposure to a variety of solvents. Figure 3c displays the changes in the values of n_{eff} after exposure to various solvents. The changes in appearance and values of n_{eff} indicated that the tethered PSt layer allowed the 2DPCG structure to sense the VOC species. This versatile process is particularly amenable to the fabrication of large-area uniform layers on solid-support surfaces with precise control over the thickness and optical properties.

In addition to applications as sensors, polymer brushes grafted from solid supports can be used as non-biofouling surfaces. Again, SI RDRP allows the grafting of concentrated polymer brushes (CPBs) from surfaces that had previously been resistant to conventional grafting-to methods.[11] The graft density of CPB is typically one order of magnitude higher than that of a semi-dilute polymer brush (SDPB) prepared through conventional methods; therefore, the CPB can display a unique structure and properties that are markedly different from those of the SDPB. Unlike the SDPB, the highly stretched CPB displayed strong repulsion against compression, superlubrication and a size-exclusion effect.[42] Using SI ATRP, three types of CPB (poly(2-hydroxyethyl methacrylate) (PHEMA), poly(2-hydroxyethyl acrylate) (PHEA) and poly(poly(ethylene glycol) methyl ether methacrylate) (PPEGMA)) were added to solid supports at various graft densities and thicknesses to allow an evaluation of their protein adsorption and cell-adhesion behavior.[43] To verify the size-exclusion ability, the adsorption of various proteins (bradykinin, insulin, bovine serum albumin, immunoglobulin and fibronectin) on the PHEMA PHEA, and PPEGMA polymer brushes was examined using a quartz crystal microbalance. As revealed in Figure 4a, the CPBs of all three polymers (that is, graft density > 0.1 chains per nm^2 with thicknesses of 2 and 10 nm) displayed very low adsorption for the five proteins when compared with that of the bare SiO_2 surfaces. This behavior was conceivably due to the size-exclusion ability of the CPBs; namely, each of the five proteins (size: R_g) was larger than the average distance between the graft points. In the cases of SDPBs that had been decorated using the grafting-to method, significant adsorption occurred (for example, by fibronectin for the SDPB of PHEMA; by bradykinin and bovine serum albumin for the SDPBs of PHEA and PPEGMA). Thus, the size-exclusion ability of the SDPBs was poorer than that of the CPBs; notably, each protein has its own anisotropic shape that might enhance its penetration through the SDPB layer, leading to irreversible adhesion. The HUVEC adhesion tests were performed on the SDPB and CPB samples and were compared with the results obtained using tissue culture polystyrene. HUVECs (10 000 cells per cm^2) were seeded on the samples and then incubated for 1 and 4 days. HUVECs were also seeded at 2500 cells per cm^2 and incubated for 7 days. The average numbers of adherent HUVECs were estimated from fluorescent images after 4',6-diamidino-2-phenylindole staining. Figure 4b displays the results after 1, 4 and 7 days. Significant HUVEC adhesion occurred on all of the SDPB samples, as well as on the tissue culture polystyrene. By contrast, all of the CPB samples

(except for the PHEMA-CPB with a thickness of 2 nm) suppressed HUVEC adhesion. These results can be comprehended by considering the protein non-adhesion of the CPB samples described above. The CPB samples of various thicknesses suppressed protein and HUVEC adsorption, possibly due to size-exclusion ability within the brush layers and the outer surfaces. By contrast, for the SDPB samples,

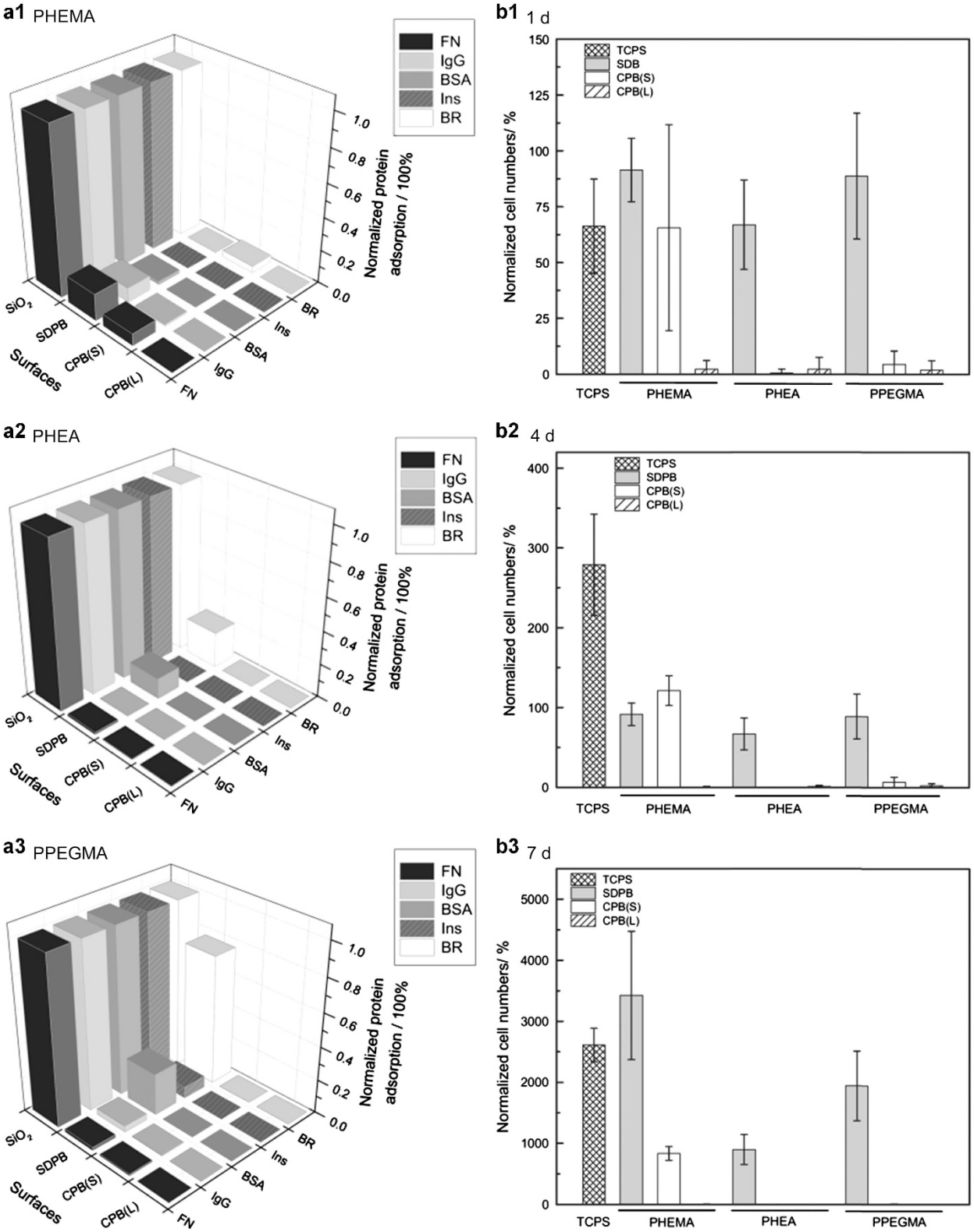

Figure 4 (**a**) Normalized amounts of irreversibly adsorbed proteins on (**a1**) PHEMA, (**a2**) PHEA and (**a3**) PPEGMA brushes on a SiO_2 surface (total cell number was normalized to the initial seeded cell number). (**b**) Normalized amounts of adherent HUVECs on the brushes after (**b1**) 1, (**b2**) 4 and (**b3**) 7 days.

the repellency between the protein and outermost brush surface decreased, suggesting that the interaction between the protein and SDPB was affected by the chemical composition. In sum, non-ionic CPB with low hydrophilicity (for example, PHEMA) has low-biofouling property and non-ionic CPB with high hydrophilicity (for example, PHEA and PPEGMA) can create ultralow-biofouling surfaces. Namely, the high graft density and hydrophilicity of non-ionic polymer brushes are important to achieve non-biofouling surfaces.

In complete contrast to non-biofouling surfaces, we used a combination of electrospinning and SI ATRP to prepare core/shell fibers possessing shortened PSt fibers (cores) and concentrated poly (sodium styrene sulfonate) brushes (shells) in another study.[44] With these biocompatible poly(sodium styrene sulfonate) brushes, the unique core/shell nanofibers were candidates for application as cell growth scaffolds.

HIGH-PERFORMANCE ADSORBENTS FROM RENEWABLE RESOURCES

In the field of environmental remediation, the development of high-performance materials—capable of removing toxic waste from soil, groundwater, sediment or surface water—from cost-effective renewable resources is an important issue affecting both daily life and industrial productivity. Table 1 lists commonly reported adsorbents for pollutants in wastewater. A variety of polysaccharide resources and their derivatives with low-cost, eco-friendly and renewable characteristics are currently the focus.

Cellulose is the most abundant biomass feedstock. Nanosized cellulose is an alternative commercial candidate for wastewater remediation. Isogai *et al.*[26] demonstrated a rapid and efficient TEMPO-mediated oxidation procedure for cellulose. As displayed in Figure 5a, the C6 primary OH group was oxidized to a carboxylate group, via an aldehyde intermediate, using two equivalents of NaClO.[60] Accordingly, an abundance of anionic carboxylate groups was introduced on the cellulose surface, providing repulsive forces among the cellulose fibers that converted the native cellulose pulp ($D_{avg} > 20\ \mu m$) to TEMPO-oxidized pulp (TOP; $D_{avg} < 20$ nm). The TOP (Figure 5b) was applied to remove paraquat—a common herbicide in agriculture, but extremely toxic to humans—from water.

Table 1 Literatures of wastewater remediation from various catalogs of general adsorbents

Adsorbents	*Pollutants*	*References*
Activated carbons	Cr^{6+}	(45)
	Benzoic acid	(46)
	Dyes	(47)
	Pb^{2+}, Cd^{2+}	(48)
	Chlorinated aromatics	(49)
Zeolites	Pb^{2+}, Cu^{2+}, Cd^{2+}	(50)
	Pb^{2+}, Cr^{3+}, Cu^{2+}, Fe^{2+}	(51)
Silica beads	Pb^{2+}, Cd^{2+}	(52)
	Dyes	(53)
Polysaccharide resources		
Saw–dust, Wheat straw	Dyes	(54,55)
Algae gelidium	Cr^{3+}, Zn^{2+}	(56)
Sugar beet pulp	Cd^{2+}, Pb^{2+}	(57)
Papermill sludge	Aromatics	(58)
Alginate/chitosan bead	Hg^{2+}	(59)

Figures 5b and c reveal the high efficiency and capacity of TOP to remove paraquat from water. Commercial granular activated carbon (GAC), a common adsorbent,[61] was also examined to compare its adsorption capacity for paraquat$_{(aq)}$. The adsorption efficiency of GAC was much lower than that of TOP (Figure 5b), presumably because of the lower number of functional groups on the GAC surface. Thus, TOP is a promising and effective adsorbent for treating wastewater contaminated with paraquat.

With the effective approach of SI RDRPs, Carlmark and Malmstrom successfully conducted SI ATRP of methyl acrylate[62] and sequential SI ATRP of methyl acrylate and HEMA[63] from the initiating sites of filter papers to obtain well-defined PMA-grafted and PMA-*b*-PHEMA-grafted (co)polymer chains that significantly decreased the paper wettability, and they further fabricated dual-responsive cellulose surfaces through SI ATRP of *N*-isopropylacrylamide and 4-vinylpyridine.[64] Perrier and colleagues performed SI RAFT polymerization with St[65] and 2-(dimethylamino)ethyl methacrylate[66] from filter papers with a chain transfer agent to obtain a hydrophobic and an antibacterial paper surface, respectively. Several other approaches using SI RDRPs with one or two monomer(s) from cellulose materials have been achieved (summarized in Table 2). Furthermore, we first demonstrated the utilization of SI ATRP and TEMPO-mediated oxidation for dual-adsorbing chlorinated aromatics and heavy metal ions, which have become a lethal issue in wastewater due to their high toxicity and non-biodegradability.

To further develop dual adsorbents, as displayed in Figure 6a, ATRP initiating sites were immobilized onto TEMPO-oxidized cellulose (named as TOCN) surface through acylation of the TOCN bundle surface.[82,83] The TOCN-Br samples with ATRP initiating sites were then used for SI ATRP (that is, step (ii) in Figure 6a) to perform the grafting-from process. Electron spectroscopy for chemical analysis allowed deconvolution of the C1s peaks[84] of cellulose, TOCN and TOCN-Br, revealing that the signal of the OH groups decreased, whereas that of the C=O groups increased, after the oxidation and acylation processes. Elemental analysis indicated a Br atom content of approximately 1–2 initiating sites in every 5–10 glucose units. After the TEMPO-mediated oxidization and acylation reactions, sodium salts of the acid groups were obtained that were inert toward Cu complexes, thereby preserving the integrity of the activation/deactivation process. A screening initiator, 2-hydroxyethyl 2-bromoisobutyrate (HEBiB), was added to the reaction medium. SI ATRP was performed with St/HEBiB/CuBr/PMDETA = 300/1/1/1 and TOCN-Br ($[St]_0 = 4.2$ M in anisole at 90 °C). Molecular weight evolution, a high molecular weight product ($M_n \approx 21$ k), and narrow unimodal GPC peaks (polydispersity ($Đ$) $\leqslant 1.1$) were observed for the reaction, indicative of successful living polymerization in the presence of TOCN with neutral carboxylic acid sodium salt groups. As confirmed by the Fourier transform infrared spectroscopy analyses, different PSt grafting contents with dilute polymer brushes (graft density (σ) < 0.01 chains per nm^2) and semi-dilute polymer brushes ($0.01 < \sigma < 0.1$ chains per nm^2) can be obtained. The CA analyses showed that the TOCN-*g*-PSt samples possess hydrophobicity, with CAs in the range 85°–98°. The increases in CAs were consistent with the graft density and chain length.

We tested the dual-functional TOCN-*g*-PSt nanomaterials for the removal of persistent organic pollutants and heavy metal ions. First, we used UV–Vis spectroscopy to monitor the adsorption profiles of the TOCN nanomaterials toward 1,2,4-trichlorobenzene (1,2,4-TCB). TOCN-*g*-PSt ($M_n = 29\,000$; $Đ = 1.13$; PSt = 12.7 wt%; $\sigma = 0.003$ chains per nm^2). Unmodified TOCN was dispersed in an aqueous solution with 1,2,4-TCB. Figure 6b shows that the concentration of 1,2,4-TCB adsorption by the unmodified TOCN was lower than that when

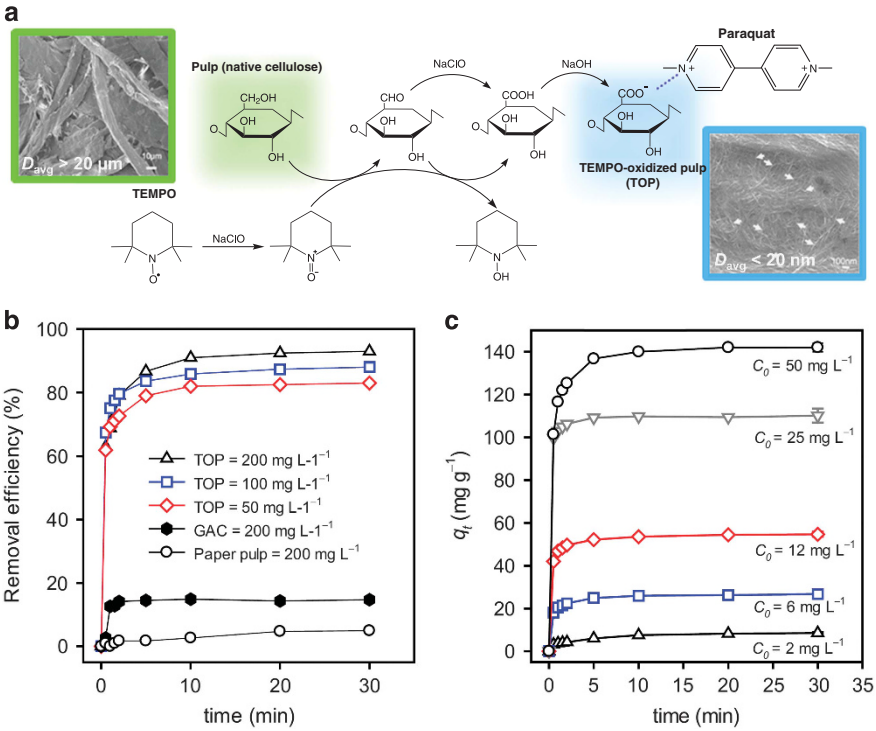

Figure 5 (**a**) Preparation of TEMPO-oxidized pulp as a high-performance adsorbent for paraquat. (**b**, **c**) Effects of (**b**) various TOP loadings on the removal efficiency (paraquat$_{(aq)}$ was initially fixed (C_0) at 5 mg l^{-1}; GAC (100 mesh)) and (**c**) various paraquat loadings on the adsorption capacity (TOP was initially fixed to 200 mg l^{-1}).

Table 2 Literatures of SI RDRPs and related surface modifications from cellulose materials

Cellulose materials	*Modification methods*	*Functional groups/Grafted polymers*	*Properties and applications*	*References*
Filter papers	SI ATRP	PMA, PMA-*b*-PHEMA, PMMA, PGMA	Hydrophobicity	(62,63,67,68)
		PNIPAAm-*b*-P4VP	Dual-responsive	(64)
	SI RAFT	P(NIPAAm-*co*-DEAAm)	Thermo-responsive	(69)
	SI SET-LRP	PCBAA	Non-fouling	(70)
	SI RAFT	PSt	Hydrophobicity	(65)
		PDMAEMA	Antibacterial	(66,71)
Jute fibers	SI ATRP	PSt	Reinforcement	(72)
Wood pulps	SI ATRP	PDMAEMA	pH-responsive	(73)
Microfibril cellulose (MFC)	SI ATRP	PBA	Reinforcement	(74,75)
	SI ATRP	PSt, PMMA, PMAm, PAcM	Dye-absorption	(76)
	SI SET-LRP	PBMA	Oil-absorption	(77)
Bacterial cellulose (BC)	SI ATRP	PMMA, PBA, P(MMA-*co*-BA)	Nanocomposites	(31)
	TO	COO^-Na^+	Nanosized fibers with wrinkled surfaces	(78,79)
Microcrystal cellulose (MCC)	SI ATRP	PSt, PMMA, PMMA-*b*-PSt	Well-dispersed in organic solvents	(80)
	Acylation	2-bromoisobutyryl	MCC macroinitiator	(81)
Nanocrystal cellulose (NCC)	SI ATRP	PSt	Nanosized fibers, liquid crystalline phase	(33)
Wood pulps	TO and SI ATRP	COO^-Na^+ and PSt	Nanosized fibers, dual-adsorbent	(82,83)

Abbreviations: PAcM, poly(acrylomorpholine); PB(M)A, poly(*n*-butyl (meth)acrylate); PCBAA, poly(carboxybetaine acrylamide); PDEAAm, poly(*N*,*N*-diethylacrylamide); PDMAEMA, poly(2-(dimethylamino)ethyl methacrylate); PGMA, poly(glycidyl methacrylate); PMAm, poly(methacrylamide); SI SET-LRP, surface-initiated single electron transfer living radical polymerization; TO, TEMPO-mediated oxidation.

employing TOCN-*g*-PSt. Under similar conditions for 2 h, the unmodified TOCN possessed lesser ability to adsorb the 1,2,4-TCB pollutant. Because many carboxylate groups were present on the nanocellulose surfaces after TEMPO-mediated oxidation, we expected that our materials would be efficient adsorbents for metal ions through ion exchange or binding to chelating sites. Figure 6c displays the data for the adsorption of Cr^{3+} and Cu^{2+} ions onto samples of cellulose, unmodified TOCN and TOCN-*g*-PSt. The native cellulose exhibited high capacities for the binding of Cr^{3+} and Cu^{2+} (*ca.* 250 and 180 mg g^{-1}, respectively). Overall, the adsorption of the Cr^{3+} and Cu^{2+} ions on the TOCN and TOCN-*g*-PSt nanocelluloses was dramatically improved compared with that of the native cellulose.

Three steps generally occur during adsorption of a pollutant onto a solid adsorbent: (i) diffusion from the solution to the interface; (ii) sorption on the adsorbent surface; and (iii) absorption into the sorbent. In our systems, prepared through a combination of

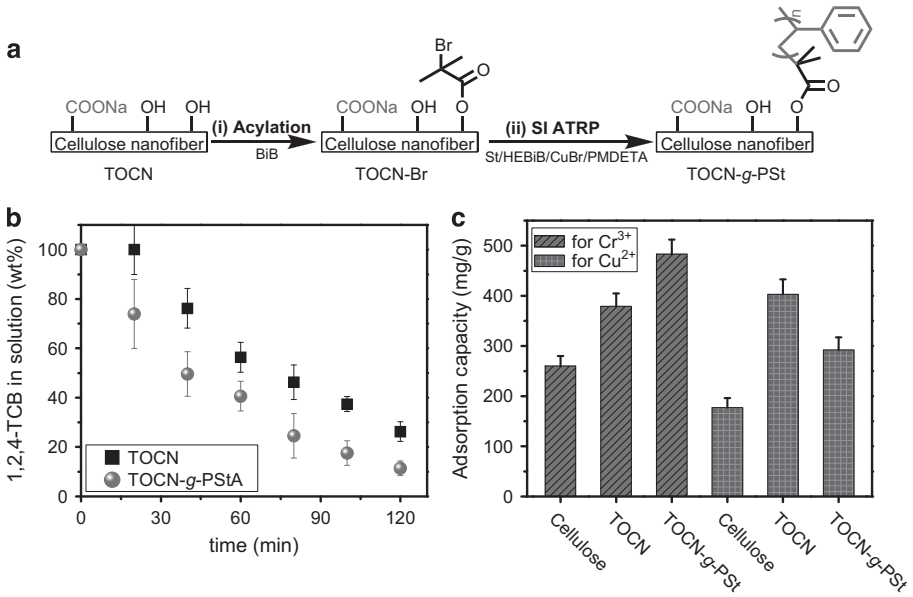

Figure 6 (**a**) Surface modifications: (i) acylation (BiB: 2-bromoisobutyryl bromide) and (ii) SI ATRP of St. (**b**, **c**) Adsorption capacities of (nano)celluloses and TOCN-*g*-PSt samples toward: (**b**) 1,2,4-TCB adsorption and (**c**) metal ions adsorption. A full color version of this figure is available at *Polymer Journal* online.

TEMPO-mediated oxidation and SI ATRP, the outer polymeric chains of the nanomaterials gathered organic (aromatic) compounds through π–π interactions, whereas the inner carboxylate groups captured metal ions through Lewis acid–base interactions.[82] This approach is amenable to provide a diverse array of nanomaterials for water remediation through pollutant removal.

SUMMARY

SI ATRP and VLSI processing are combined to fabricate surface-patterned PMMA and PSt brushes on Si wafers. The PSt brush layer displayed significant solvent-responsive behavior and could be extended to application as a VOC sensor. In addition, the preparations of CPB and SDPB layers can also be controlled readily through SI ATRP. Based on the biocompatibility of the tethered polymer chains, either a non-biofouling surface or a cell-growing scaffold could be designed. Non-ionic CPB with low hydrophilicity (for example, PHEMA) has low-biofouling properties, and non-ionic CPB with high hydrophilicity (for example, PHEA and PPEGMA) can produce ultralow-biofouling surfaces. Namely, high graft density and hydrophilicity of non-ionic polymer brushes are the keys to non-biofouling surfaces. Renewable polysaccharides of celluloses can be used for environmental remediation. After TEMPO-mediated oxidation, TEMPO-oxidized cellulose pulp displayed superior adsorption properties for the removal of paraquat. With further use of SI ATRP of St from oxidized nanocellulose, novel TOCN-*g*-PSt materials were obtained with unique dual-adsorption properties toward 1,2,4-TCB and heavy metal ions. In summary, we have presented several facile synthetic approaches—using SI ATRP and TEMPO-mediated oxidizations—for the preparation of functional surfaces and have demonstrated their effectiveness when combined with contemporary lithography process.

CONFLICT OF INTEREST

The author declares no conflict of interest.

ACKNOWLEDGEMENTS

C-F Huang thanks the Ministry of Science and Technology (MOST104-2221-E-005-088, MOST104-2923-E-194-001 and MOST104-2218-E-005-006) for financial support.

1 Hadjichristidis, N., Pitsikalis, M., Pispas, S. & Iatrou, H. Polymers with complex architecture by living anionic polymerization. *Chem. Rev.* **101**, 3747–3792 (2001).
2 Ito, S., Goseki, R., Ishizone, T. & Hirao, A. Synthesis of well-controlled graft polymers by Living anionic polymerization towards exact graft polymers. *Polym. Chem.* **5**, 5523–5534 (2014).
3 Sawamoto, M. Modern cationic vinyl polymerization. *Prog. Polym. Sci.* **16**, 111–172 (1991).
4 Yagci, Y. & Reetz, I. Externally stimulated initiator systems for cationic polymerization. *Prog. Polym. Sci.* **23**, 1485–1538 (1998).
5 Braunecker, W. A. & Matyjaszewski, K. Controlled/living radical polymerization: features, developments, and perspectives. *Prog. Polym. Sci.* **32**, 93–146 (2007).
6 Sugi, R., Yokoyama, A., Furuyama, T., Uchiyama, M. & Yokozawa, T. Inductive effect-assisted chain-growth polycondensation. Synthetic development from para- to meta-substituted aromatic polyamides with low polydispersities. *J. Am. Chem. Soc.* **127**, 10172–10173 (2005).
7 Yokozawa, T., Ogawa, M., Sekino, A., Sugi, R. & Yokoyama, A. Chain-growth polycondensation for well-defined aramide. Synthesis of unprecedented block copolymer containing aramide with low polydispersity. *J. Am. Chem. Soc.* **124**, 15158–15159 (2002).
8 Bielawski, C. W. & Grubbs, R. H. Living ring-opening metathesis polymerization. *Prog. Polym. Sci.* **32**, 1–29 (2007).
9 Mecerreyes, D., Jerome, R. & Dubois, P. Novel macromolecular architectures based on aliphatic polyesters: relevance of the "coordination-insertion" ring-opening polymerization. *Adv. Polym. Sci.* **147**, 1–59 (1999).
10 Dong, H., Zhu, M., Yoon, J. A., Gao, H., Jin, R. & Matyjaszewski, K. One-pot synthesis of robust core/shell gold nanoparticles. *J. Am. Chem. Soc.* **130**, 12852–12853 (2008).
11 Ohno, K., Morinaga, T., Koh, K., Tsujii, Y. & Fukuda, T. Synthesis of monodisperse silica particles coated with well-defined, high-density polymer brushes by surface-initiated atom transfer radical polymerization. *Macromolecules* **38**, 2137–2142 (2005).
12 Parvole, J., Montfort, J. P., Reiter, G., Borisov, O. & Billon, L Elastomer polymer brushes on flat surface by bimolecular surface-initiated nitroxide mediated polymerization. *Polymer* **47**, 972–981 (2006).
13 Tsujii, Y., Ejaz, M., Sato, K., Goto, A. & Fukuda, T. Mechanism and kinetics of RAFT-mediated graft polymerization of styrene on a solid surface. 1. Experimental evidence of surface radical migration. *Macromolecules* **34**, 8872–8878 (2001).
14 Ying, L., Yu, W. H., Kang, E. T. & Neoh, K. G. Functional and surface-active membranes from poly(vinylidene fluoride)-graft-poly(acrylic acid) prepared via RAFT-mediated graft copolymerization. *Langmuir* **20**, 6032–6040 (2004).
15 Wang, L.-P., Dong, L.-H., Hao, J.-C., Lv, X.-H., Li, W.-Z., Li, Y.-C., Zhen, J.-M., Hao, Y.-C. & Ma, F. Fabrication of block copolymer brushes on hollow sphere surface

via reverse iodine transfer polymerization. *J. Colloid Interface Sci.* **361**, 400–406 (2011).
16 Yamago, S., Yahata, Y., Nakanishi, K., Konishi, S., Kayahara, E., Nomura, A., Goto, A. & Tsujii, Y. Synthesis of concentrated polymer brushes via surface-initiated organotellurium-mediated living radical polymerization. *Macromolecules* **46**, 6777–6785 (2013).
17 Hucknall, A., Simnick, A. J., Hill, R. T., Chilkoti, A., Garcia, A., Johannes, M. S., Clark, R. L., Zauscher, S. & Ratner, B. D. Versatile synthesis and micropatterning of nonfouling polymer brushes on the wafer scale. *Biointerphases* **4**, Fa50–Fa57 (2009).
18 Lavanant, L., Pullin, B., Hubbell, J. A. & Klok, H. A. A facile strategy for the modification of polyethylene substrates with non-fouling, bioactive poly(poly(ethylene glycol) methacrylate) brushes. *Macromol. Biosci.* **10**, 101–108 (2010).
19 Yu, Q. A., Zhang, Y. X., Wang, H. W., Brash, J. & Chen, H. Anti-fouling bioactive surfaces. *Acta Biomater.* **7**, 1550–1557 (2011).
20 Barbey, R., Lavanant, L., Paripovic, D., Schuewer, N., Sugnaux, C., Tugulu, S. & Klok, H.-A. Polymer brushes via surface-initiated controlled radical polymerization: synthesis, characterization, properties, and applications. *Chem. Rev.* **109**, 5437–5527 (2009).
21 Matyjaszewski, K. & Tsarevsky, N. V. Nanostructured functional materials prepared by atom transfer radical polymerization. *Nat. Chem.* **1**, 276–288 (2009).
22 Lee, H.-I., Pietrasik, J., Sheiko, S. S. & Matyjaszewski, K. Stimuli-responsive molecular brushes. *Prog. Polym. Sci.* **35**, 24–44 (2010).
23 Motornov, M., Roiter, Y., Tokarev, I. & Minko, S. Stimuli-responsive nanoparticles, nanogels and capsules for integrated multifunctional intelligent systems. *Prog. Polym. Sci.* **35**, 174–211 (2010).
24 Hucknall, A., Rangarajan, S. & Chilkoti, A. In pursuit of zero: polymer brushes that resist the adsorption of proteins. *Adv. Mater.* **21**, 2441–2446 (2009).
25 Brittain, W. J., Boyes, S. G., Granville, A. M., Baum, M., Mirous, B. K., Akgun, B., Zhao, B., Blickle, C. & Foster, M. D. Surface rearrangement of diblock copolymer brushes - stimuli responsive films. *Adv. Polym. Sci.* **198**, 125–147 (2006).
26 Isogai, A., Saito, T. & Fukuzumi, H. TEMPO-oxidized cellulose nanofibers. *Nanoscale* **3**, 71–85 (2011).
27 Goffin, A. L., Raquez, J. M., Duquesne, E., Siqueira, G., Habibi, Y., Dufresne, A. & Dubois, P. Poly(epsilon-caprolactone) based nanocomposites reinforced by surface-grafted cellulose nanowhiskers via extrusion processing: morphology, rheology, and thermo-mechanical properties. *Polymer* **52**, 1532–1538 (2011).
28 Goffin, A.-L., Raquez, J.-M., Duquesne, E., Siqueira, G., Habibi, Y., Dufresne, A. & Dubois, P. From interfacial ring-opening polymerization to melt processing of cellulose nanowhisker-filled polylactide-based nanocomposites. *Biomacromolecules* **12**, 2456–2465 (2011).
29 Habibi, Y., Aouadi, S., Raquez, J.-M. & Dubois, P. Effects of interfacial stereocomplexation in cellulose nanocrystal-filled polylactide nanocomposites. *Cellulose* **20**, 2877–2885 (2013).
30 Habibi, Y., Goffin, A.-L., Schiltz, N., Duquesne, E., Dubois, P. & Dufresne, A. Bionanocomposites based on poly(epsilon-caprolactone)-grafted cellulose nanocrystals by ring-opening polymerization. *J. Mater. Chem.* **18**, 5002–5010 (2008).
31 Lacerda, P. S., Barros-Timmons, A. M., Freire, C. S., Silvestre, A. J. & Neto, C. P. Nanostructured composites obtained by ATRP sleeving of bacterial cellulose nanofibers with acrylate polymers. *Biomacromolecules* **14**, 2063–2073 (2013).
32 Morandi, G., Heath, L. & Thielemans, W. Cellulose nanocrystals grafted with polystyrene chains through surface-initiated atom transfer radical polymerization (SI-ATRP). *Langmuir* **25**, 8280–8286 (2009).
33 Yi, J., Xu, Q., Zhang, X. & Zhang, H. Chiral-nematic self-ordering of rodlike cellulose nanocrystals grafted with poly(styrene) in both thermotropic and lyotropic states. *Polymer* **49**, 4406–4412 (2008).
34 Prime, K. L. & Whitesides, G. M. Adsorption of proteins onto surfaces containing end-attached oligo(ethylene oxide) - a model system using self-assembled monolayers. *J. Am. Chem. Soc.* **115**, 10714–10721 (1993).
35 Chen, J.-K., Hsieh, C.-Y., Huang, C.-F., Li, P.-M., Kuo, S.-W. & Chang, F.-C. Using solvent immersion to fabricate variably patterned poly(methyl methacrylate) brushes on silicon surfaces. *Macromolecules* **41**, 8729–8736 (2008).
36 Zhao, B. & Brittain, W. J. Polymer brushes: surface-immobilized macromolecules. *Prog. Polym. Sci.* **25**, 677–710 (2000).
37 Ganesh, V. A., Baji, A. & Ramakrishna, S. Smart functional polymers - a new route towards creating a sustainable environment. *RSC Adv.* **4**, 53352–53364 (2014).
38 Welch, M. E. & Ober, C. K. Responsive and patterned polymer brushes. *J. Polym. Sci. B Polym. Phys.* **51**, 1457–1472 (2013).
39 Chen, J.-K. & Chang, C.-J. Fabrications and applications of stimulus-responsive polymer films and patterns on surfaces: a review. *Materials* **7**, 805–875 (2014).
40 Chen, J.-K., Hsieh, C.-Y., Huang, C.-F. & Li, P.-M. Characterization of patterned poly(methyl methacrylate) brushes under various structures upon solvent immersion. *J. Colloid Interface Sci.* **338**, 428–434 (2009).
41 Chen, J. K., Wang, J. H., Chang, C. J. & Huang, C. F. Polarity-indicative two-dimensional periodic concave gratings of tethered polystyrene on silicon surfaces for visualization in VOC sensing. *Sensor. Actuators B Chem.* **188**, 1123–1131 (2013).
42 Yoshikawa, C., Hattori, S., Honda, T., Huang, C. F. & Kobayashi, H. Non-biofouling property of well-defined concentrated poly(2-hydroxyethyl methacrylate) brush. *Mater. Lett.* **83**, 140–143 (2012).
43 Yoshikawa, C., Qiu, J., Huang, C. F., Shimizu, Y., Suzuki, J. & van den Bosch, E. Non-biofouling property of well-defined concentrated polymer brushes. *Colloids Surf. B Biointerfaces* **127**, 213–220 (2015).
44 Huang, C. F., Yoshikawa, C., Zhang, K., Hattori, S., Honda, T., Zawadzak, E. & Kobayashi, H. Fabrication of shortened electrospun fibers with concentrated polymer brush toward biomaterial applications. *Adv. Mater. Res.* **306-307**, 58–62 (2011).
45 Xiao, Y., Ge, M., Xue, X., Wang, C., Wang, H., Wu, X., Li, L., Liu, L., Qi, X., Zhang, Y., Li, Y., Luo, H., Xie, T., Gu, J. & Ren, J. Hepatic cytochrome P450s metabolize aristolochic acid and reduce its kidney toxicity. *Kidney Int.* **73**, 1231–1239 (2008).
46 Chern, J. M. & Chien, Y. W. Competitive adsorption of benzoic acid and p-nitrophenol onto activated carbon: isotherm and breakthrough curves. *Water Res.* **37**, 2347–2356 (2003).
47 Pereira, M. F. R., Soares, S. F., Orfao, J. J. M. & Figueiredo, J. L. Adsorption of dyes on activated carbons: influence of surface chemical groups. *Carbon* **41**, 811–821 (2003).
48 Rivera-Utrilla, J., Bautista-Toledo, I., Feffo-Garcia, M. A. & Moreno-Castilla, C. Bioadsorption of Pb(II), Cd(II), and Cr(VI) on activated carbon from aqueous solutions. *Carbon* **41**, 323–330 (2003).
49 Jung, M. W., Ahn, K. H., Lee, Y., Kim, K. P., Rhee, J. S., Park, J. T. & Paeng, K. J. Adsorption characteristics of phenol and chlorophenols on granular activated carbons (GAC). *Microchem. J.* **70**, 123–131 (2001).
50 Bosso, S. T. & Enzweiler, J. Evaluation of heavy metal removal from aqueous solution onto scolecite. *Water Res.* **36**, 4795–4800 (2002).
51 Inglezakis, V. J., Loizidou, M. D. & Grigoropoulou, H. P. Ion exchange of Pb^{2+}, Cu^{2+}, Fe^{3+}, and Cr^{3+} on natural clinoptilolite: selectivity determination and influence of acidity on metal uptake. *J. Colloid Int. Sci.* **261**, 49–54 (2003).
52 Ghoul, M., Bacquet, M. & Morcellet, M. Uptake of heavy metals from synthetic aqueous solutions using modified PEI - silica gels. *Water Res.* **37**, 729–734 (2003).
53 Krysztafkiewicz, A., Binkowski, S. & Jesionowski, T. Adsorption of dyes on a silica surface. *Appl. Surf. Sci.* **199**, 31–39 (2002).
54 Garg, V. K., Gupta, R., Yadav, A. B. & Kumar, R. Dye removal from aqueous solution by adsorption on treated sawdust. *Biores. Tech.* **89**, 121–124 (2003).
55 Robinson, T., Chandran, B. & Nigam, P. Removal of dyes from a synthetic textile dye effluent by biosorption on apple pomace and wheat straw. *Water Res.* **36**, 2824–2830 (2002).
56 Vilar, V. J. P., Botelho, C. M. S. & Boaventura, R. A. R. Chromium and zinc uptake by algae Gelidium and agar extraction algal waste: kinetics and equilibrium. *J. Hazard Mater.* **149**, 643–649 (2007).
57 Reddad, Z., Gerente, C., Andres, Y., Thibault, J. F. & Le Cloirec, P. Cadmium and lead adsorption by a natural polysaccharide in MF membrane reactor: experimental analysis and modelling. *Water Res.* **37**, 3983–3991 (2003).
58 Calace, N., Nardi, E., Petronio, B. M. & Pietroletti, M. Adsorption of phenols by papermill sludges. *Environ. Pollut.* **118**, 315–319 (2002).
59 Chang, Y.-H., Huang, C.-F., Hsu, W.-J. & Chang, F.-C. Removal of Hg^{2+} from aqueous solution using alginate gel containing chitosan. *J. Appl. Polym. Sci.* **104**, 2896–2905 (2007).
60 Lin, K. Y. A., Heish, Y. T., Tsai, T. Y. & Huang, C. F. TEMPO-oxidized pulp as an efficient and recyclable sorbent to remove paraquat from water. *Cellulose* **22**, 3261–3274 (2015).
61 Gupta, V. K., Gupta, B., Rastogi, A., Agarwal, S. & Nayak, A. Pesticides removal from waste water by activated carbon prepared from waste rubber tire. *Water Res.* **45**, 4047–4055 (2011).
62 Carlmark, A. & Malmstrom, E. Atom transfer radical polymerization from cellulose fibers at ambient temperature. *J. Am. Chem. Soc.* **124**, 900–901 (2002).
63 Carlmark, A. & Malmstrom, E. E. ATRP grafting from cellulose fibers to create block-copolymer grafts. *Biomacromolecules* **4**, 1740–1745 (2003).
64 Lindqvist, J., Nystrom, D., Ostmark, E., Antoni, P., Carlmark, A., Johansson, M., Hult, A. & Malmstrom, E Intelligent dual-responsive cellulose surfaces via surface-initiated ATRP. *Biomacromolecules* **9**, 2139–2145 (2008).
65 Roy, D., Guthrie, J. T. & Perrier, S. Graft polymerization: grafting poly(styrene) from cellulose via reversible addition-fragmentation chain transfer (RAFT) polymerization. *Macromolecules* **38**, 10363–10372 (2005).
66 Roy, D., Knapp, J. S., Guthrie, J. T. & Perrier, S. Antibacterial cellulose fiber via RAFT surface graft polymerization. *Biomacromolecules* **9**, 91–99 (2008).
67 Hansson, S., Antoni, P., Bergenudd, H. & Malmstrom, E. Selective cleavage of polymer grafts from solid surfaces: assessment of initiator content and polymer characteristics. *Polym. Chem.* **2**, 556–558 (2011).
68 Hansson, S., Ostmark, E., Carlmark, A. & Malmstrom, E. ARGET ATRP for versatile grafting of cellulose using various monomers. *ACS Appl. Mater. Inter.* **1**, 2651–2659 (2009).
69 Hufendiek, A., Trouillet, V., Meier, M. A. R. & Barner-Kowollik, C. Temperature responsive cellulose-graft-copolymers via cellulose functionalization in an ionic liquid and RAFT polymerization. *Biomacromolecules* **15**, 2563–2572 (2014).
70 Tischer, T., Rodriguez-Emmenegger, C., Trouillet, V., Welle, A., Schueler, V., Mueller, J. O., Goldmann, A. S., Brynda, E. & Barner-Kowollik, C. Photo-patterning of non-fouling polymers and biomolecules on paper. *Adv. Mater.* **26**, 4087–4092 (2014).
71 Roy, D., Guthrie, J. T. & Perrier, S. RAFT graft polymerization of 2-(dimethylaminoethyl) methacrylate onto cellulose fiber. *Aus. J. Chem.* **59**, 737–741 (2006).
72 Plackett, D., Jankova, K., Egsgaard, H. & Hvilsted, S. Modification of jute fibers with polystyrene via atom transfer radical polymerization. *Biomacromolecules* **6**, 2474–2484 (2005).
73 Sui, X. F., Yuan, J. Y., Zhou, M., Zhang, J., Yang, H. J., Yuan, W. Z., Wei, Y. & Pan, C. Y. Synthesis of cellulose-graft-poly(*N,N*-dimethylamino-2-ethyl methacrylate) copolymers via homogeneous ATRP and their aggregates in aqueous media. *Biomacromolecules* **9**, 2615–2620 (2008).
74 Li, S. Z., Xiao, M. M., Zheng, A. & Xiao, H. N. Cellulose microfibrils grafted with PBA via surface-initiated atom transfer radical polymerization for biocomposite reinforcement. *Biomacromolecules* **12**, 3305–3312 (2011).

75 Xiao, M. M., Li, S. Z., Chanklin, W., Zheng, A. N. & Xiao, H. N. Surface-initiated atom transfer radical polymerization of butyl acrylate on cellulose microfibrils. *Carbohydr. Polym.* **83**, 512–519 (2011).
76 Coskun, M. & Temuz, M. M. Grafting studies onto cellulose by atom-transfer radical polymerization. *Polym. Int.* **54**, 342–347 (2005).
77 Fan, L. J., Chen, H., Hao, Z. H. & Tan, Z. Cellulose-based macroinitiator for crosslinked poly(butyl methacrylate-*co*-pentaerythritol triacrylate) oil-absorbing materials by SET-LRP. *J. Polym. Sci. A Polym. Chem.* **51**, 457–462 (2013).
78 Lai, C., Zhang, S. J., Sheng, L. Y., Liao, S. B., Xi, T. F. & Zhang, Z. X. TEMPO-mediated oxidation of bacterial cellulose in a bromide-free system. *Colloid Polym. Sci.* **291**, 2985–2992 (2013).
79 Lai, C., Sheng, L. Y., Liao, S. B., Xi, T. F. & Zhang, Z. X. Surface characterization of TEMPO-oxidized bacterial cellulose. *Surf. Interface Anal.* **45**, 1673–1679 (2013).
80 Meng, T., Gao, X., Zhang, J., Yuan, J. Y., Zhang, Y. Z. & He, J. S. Graft copolymers prepared by atom transfer radical polymerization (ATRP) from cellulose. *Polymer* **50**, 447–454 (2009).
81 Supeno, S., Daik, R. & El-Sheikh, S. M. The synthesis of a macro-initiator from cellulose in a zinc-based ionic liquid. *Bioresources* **9**, 1267–1275 (2014).
82 Huang, C. F., Chen, J. K., Tsai, T. Y., Hsieh, Y. A. & Lin, K. Y. A. Dual-functionalized cellulose nanofibrils prepared through TEMPO-mediated oxidation and surface-initiated ATRP. *Polymer* **72**, 395–405 (2015).
83 Tsai, T. Y. & Huang, C. F. Data in support of dual-functionalized cellulose nanofibrils prepared through TEMPO-mediated oxidation and surface-initiated ATRP. *Data Brief* **3**, 195–200 (2015).
84 Zhu, S., Li, J., Chen, Y., Chen, Z., Chen, C., Li, Y., Cui, Z. & Zhang, D. Grafting of graphene oxide with stimuli-responsive polymers by using ATRP for drug release. *J. Nanopart. Res.* **14**, 1132–1142 (2012).